ELSEVIER

Contents lists available at ScienceDirect

Journal of Colloid And Interface Science

journal homepage: www.elsevier.com/locate/jcis



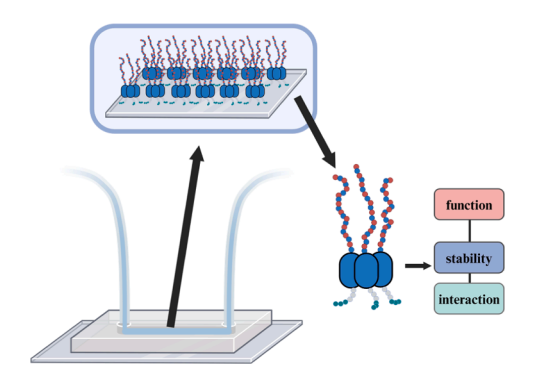


One-step antifouling coating of polystyrene using engineered polypeptides

Chuanbao Zheng ^{a,b}, Zohaib Hussain ^a, Chang Chen ^a, Robbert Jan de Haas ^a, Siddharth Deshpande ^a, Zhisen Zhang ^c, Han Zuilhof ^{b,d}, Renko de Vries ^{a,*}

- ^a Physical Chemistry and Soft Matter, Wageningen University & Research, Stippeneng 4 6708 WE Wageningen, The Netherlands
- b Laboratory of Organic Chemistry, Wageningen University & Research, Stippeneng 4 6708 WE Wageningen, The Netherlands
- ^c Research Institute for Biomimetics and Soft Matter, Fujian Provincial Key Laboratory for Soft Functional Materials Research, Department of Physics, Xiamen University 361005 Xiamen. China
- d China-Australia Institute for Advanced Materials and Manufacturing, College of Biological, Chemical Science and Engineering, Jiaxing University 314001 Jiaxing, China

GRAPHICAL ABSTRACT



ARTICLE INFO

Keywords:
Polystyrene surface
Solid-binding peptides
Antifouling
Elastin-like polypeptides
MD simulations

ABSTRACT

Unwanted nonspecific adsorption caused by biomolecules influences the lifetime of biomedical devices and the sensing performance of biosensors. Previously, we have designed B-M-E triblock proteins that rapidly assemble on inorganic surfaces (gold and silica) and render those surfaces antifouling. The B-M-E triblock proteins have a surface-binding domain B, a multimerization domain M and an antifouling domain E. Many biomedical technologies involve organic (polymeric) surfaces where B-M-E triblock proteins could potentially be used. In this study, we computationally and experimentally investigate the assembly of B-M-E triblock proteins on polystyrene (PS) surfaces, using PS-binding peptides as a surface-binding block B. We used atomic force microscopy, dynamic light scattering, fluorescence microscopy and quartz crystal microbalance to test the antifouling coating functionality. We found that, like for inorganic surfaces, the B-M-E proteins with PS-binding peptides as B block, form homogeneous monomolecular layers on PS surfaces with good stability against PBS washing. The adsorbed protein layer fully prevents adsorption of fluorescently labeled bovine serum albumin to PS microfluidic chips. Similarly, no significant fouling was observed using quartz crystal microbalance when 1 % (v/v) or 10 % (v/v) human serum were used as foulants.

E-mail address: renko.devries@wur.nl (R. de Vries).

 $^{^{\}star}$ Corresponding author.

1. Introduction

Nonspecific adsorption of unwanted foulants, like biomolecules or microorganisms, strongly influences the performance of biomedical devices and biosensing applications [1-7]. Preventing nonspecific adsorption of biomolecules (biofouling) on solid surfaces is a key challenge in numerous technologies. To make surfaces fouling resistant, antifouling coatings, including active and passive antifouling, have been developed [8,9]. While active antifouling coatings prevent fouling by actively degrading foulants using biocidal agents [10-12], whereas passive antifouling coatings merely prevent adsorption of foulants. A prime example of passive antifouling is surface modifications with hydrophilic polymer brushes [13,14]. The hydrophilic polymer brushes can be attached to surfaces by chemical (covalently) or physical (noncovalently) methods. For example, poly(ethylene glycol) or zwitterionic polymers can be covalently immobilized as brushes on multiple surfaces [15-17], such as through thiol and thiol derivatives [18-22] on gold surfaces. Physical attachment of poly(ethylene glycol) or other polymers to surfaces is often achieved using poly(l-lysine) as a surface anchoring polymer [21–23]. For example, a poly(l-lysine)-g-poly(ethylene glycol) copolymer consists of a poly(l-lysine) main chain and poly(ethylene glycol) side chains. The polycationic poly(l-lysine) main chain adsorbs to negatively charged surfaces via electrostatic interactions, while the poly(ethylene glycol) side chains form brushes that associate with the poly(l-lysine) main chain through hydrogen bonding or van der Waals interactions, resulting in a brush-like structure that provides antifouling

Sequence-designed proteins, expressed in suitable hosts such as *E. coli*, can be explored as an alternative to synthetic antifouling polymers that are physically attached to surfaces. Besides being fully biobased and biodegradable, sequence-designed proteins allow for the use of solid-binding peptides sequences as material-specific surface anchors [25]. Previously, we designed a family of coating proteins with a *B-M-E* triblock structure. The *B-M-E* designs feature a solid-binding block *B* containing a solid-binding peptide sequence [25–28], a multimerization block *M* enhancing the overall surface-binding strength through multivalency, and a hydrophilic elastin-like polypeptide block *E* providing antifouling functionality [29–31].

By employing a range of different multimerization blocks *M* in a *B-M-E* triblock, Alvisi and coworkers [32] found that many of the designs led to the formation of insoluble products, complicating the purification process. Among the various multimerization *M* blocks tested, only one *de novo* designed thermostable trimer [33] when used as the *M* block, enhanced the solubility of the *B-M-E* triblock and facilitated its expression in *E. coli. B-M-E* coating proteins with this specific *M* block were shown to rapidly assemble on inorganic surfaces including silica and gold, rendering the surfaces antifouling against serum proteins [32,34].

Here, we aim to explore the potential of **B-M-E** coating proteins to render polymeric surfaces antifouling. Many devices and sensors are made of low-cost and mechanically strong polymeric materials, especially in biomedical and biosensing applications [35–37]. At a molecular level, the atoms of polymeric material have a higher intrinsic mobility [38] than inorganic surfaces such as silica and gold. This mobility could potentially impede the long-term stability of antifouling coatings on polymeric surfaces. Another key challenge for physically adsorbed hydrophilic polymer brushes on polymeric surfaces, using coating proteins with a B-M-E triblock architecture, is the requirement for strong hydrophobic interactions to ensure effective attachment. This surface attachment process inherently involves highly hydrophobic peptide sequences as part of the **B** domain. However, these hydrophobic sequences can lead to insolubility or aggregation of the B-M-E proteins due to bridging interactions, where multiple hydrophobic tags on different B-M-E cluster together. Additionally, biomolecular foulants, such as proteins, can strongly interact with hydrophobic molecules and surfaces. These foulants may displace the coating both by interacting with the

hydrophobic B domains of the B-M-E proteins or directly interacting with the hydrophobic surface.

Strategies for the physical immobilization of polymer brushes to polymeric surfaces have also been developed based on synthetic polymer chemistry [39–41]. Here, we investigate whether the **B-M-E** triblock design can perform as effectively on polymeric surfaces by using a polymeric-surface-binding peptide as the **B** block, without altering the other blocks. Polystyrene (PS) will be used as a model polymeric surface in this study.

Even though there are many reports on polymeric-surfaces-binding peptide sequences, this has not yet led to the design of coating proteins that makes use of these peptides as surface anchors [25]. Instead, polymeric-surfaces-binding peptide sequences, such as PS-binding peptides, have mainly been used as simple material-tags for direct immobilization of target proteins on PS surfaces [42–44]. However, less attention has been given to the stability of the attachment, possible fouling of the functionalized surfaces, or to the displacement of attached proteins by foulant molecules.

Despite the difficulty in achieving comparable antifouling functionality for polymeric surfaces compared to inorganic surfaces, we present our initial results utilizing PS-binding peptides as surface anchors in protein-based, one-step antifouling coatings for PS surfaces, employing the B-M-E triblock design. We selected a PS-binding peptide with the (one letter code) amino acid sequence VHWDFRQWWQPS [44] as the B domain of our earlier **B-M-E** triblock protein [34], leaving the rest of the protein sequence unchanged. We used matrix-assisted laser desorption/ ionization time of flight (MALDI-TOF) mass spectrometry to characterize the molecular weight of the PS-binding B-M-E proteins, and circular dichroism (CD) to verify the folding of the M block within B-M-E proteins. Next, we investigate coating formation and antifouling functionality of the B-M-E proteins using quartz crystal microbalance with dissipation (QCM-D), dynamic light scattering (DLS), atomic force microscopy (AFM), atomistic molecular dynamics (MD) simulations, and PS-microfluidic chips.

2. Results and discussion

2.1. Protein design, production, and characterization

Fig. 1 presents a schematic illustration of the PS-binding *B-M-E* protein adsorbed on a PS surface. The *N*-terminal surface anchor block *B*, includes a His-tag for nickel affinity purification, a PS-binding peptide with (one-letter code) amino acid sequence VHWDFRQWWQPS) [44], and a short hydrophilic linker with three repeats of the amino acid sequence (GSGVP). Following our earlier work [32], the multimerization block *M* (HR00C_3_2) is a *de novo* designed, helical repeat protein that forms a thermostable trimer [33]. Building on our previous work on *B-M-E* proteins [34], which assemble into antifouling brushes on gold surfaces, we selected a zwitterionic elastin-like polypeptide sequence for the *E* block, consisting of ten repeats of (GDGVP-GKGVP). The *M* block has its N- and C- termini on opposite sides, such that when the N-terminal *B* block binds to the surface, the C-terminal *E* block is oriented towards the solution side, as illustrated in Fig. 1.

Primers and DNA sequences, along with complete amino acid sequences of the PS-binding **B-M-E** protein used in this study, are provided in the Supporting Information (Tables S1–S3). Genes encoding the sequences of the PS-binding **B-M-E** protein were purchased and cloned into a vector with a T7 promoter system. Proteins were expressed in **E. coli** and purified using chromatography. For more details, see Materials and Methods section. Results for the characterization of the purified **B-M-E** protein are shown in Fig. 2. The main band in SDS-PAGE indicates good purity after final SEC purification (Fig. 2a). A protein monomer with an estimated molecular weight of approximately 40 kDa was observed. MALDI-TOF results (Fig. 2b) confirmed that the molar weight of the purified **B-M-E** protein (43309.6 Da) is within 0.1 % error of the theoretical value (43289.5 Da). The two peaks in the MALDI-TOF

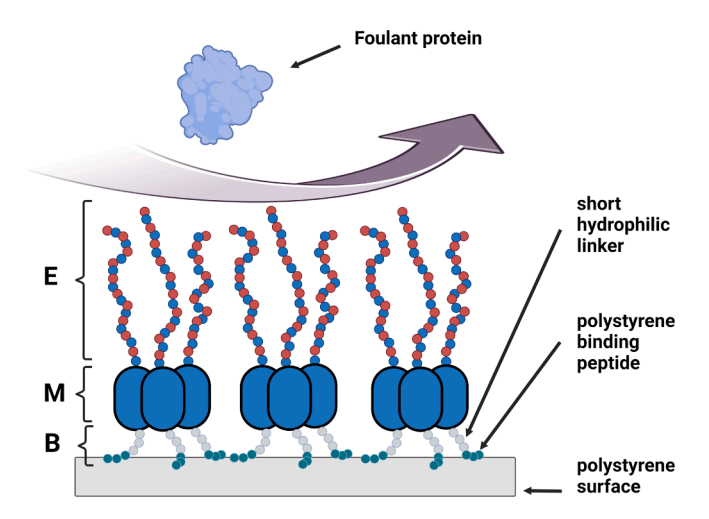


Fig. 1. Schematic representation of PS-binding B-M-E protein bound to a PS surface, preventing fouling by a foulant protein. The B domain is positioned at the N-terminus, the E domain at the C-terminus. The M domain is located between the B and E domains. For clarity, the His-tag at the N-terminus is not shown.

spectra represent (*B-M-E* with 2H)²⁺ and (*B-M-E* with H)⁺. In Fig. 2c, the retention volume of the trimeric *B-M-E* protein, with a molecular weight of approximate 130 kDa in SEC, is similar to that observed for the gold-binding version of the *B-M-E* protein, which also has an approximate molecular weight of 130 kDa [34]. These data are consistent with the molecular size expected for a *B-M-E* trimer.

Next, CD measurements were performed to confirm the correct folding of the M block within the B-M-E proteins (Fig. 2d). For the ordinate of CD data, the θ refers to the molar ellipticity (deg cm² dmol⁻¹). α -helical proteins alone showed a characteristic double dip

feature in the CD spectrum with two minima at 222 nm and 208 nm, respectively [45]. For the *B-M-E* triblock proteins, we have previously shown that the CD spectra for the gold-binding and silica-binding versions of *B-M-E* protein [32,34] are dominated by the contribution of the purely α -helical midblock M showing the characteristic minima around 222 nm and 208 nm. Therefore, we concluded that the midblock M folds correctly in the context of the *B-M-E* protein.

The temperature dependence of the CD spectra informs about thermal denaturation: above the denaturation transition, the α -helical secondary structure of the M block will be lost, and so will the minima around 222 nm and 208 nm in the CD spectra. Next, the residue molar ellipticity at 220 nm was measured by CD to assess the thermal stability of the B-M-E protein during heating from 20 °C to 95 °C (Fig. 2e). The results showed no significant signs of unfolding. Hence, we conclude that the B-M-E proteins exhibit high thermal stability against unfolding, consistent with our previous findings for the silica-binding and gold-binding B-M-E designs [32,34].

2.2. Coating formation on PS surface

Next, we tested the kinetics of **B-M-E** protein adsorption on PS surfaces using QCM-D, and the results obtained are shown in Fig. 3. First, a flat baseline was obtained by flushing the system with PBS only. The **B-M-E** proteins were then injected into the sample channel. After injection, the frequency signal decreased sharply and stabilized, indicating that the **B-M-E** proteins absorbed to the PS surface and quickly reached saturation. After that, the sample channel was rinsed with PBS again. A very slight upward trend was observed during the following PBS rinsing step, which may indicate the dissociation of a minimal amount of adsorbed **B-M-E** proteins. For completeness, the results for the QCM-D dissipation signal are shown in Fig. S1. Similar to our finding with **B-M-E** proteins on gold and silica surfaces, the hydrophilic random coiled **E** blocks contribute to significant dissipation, making it challenging to

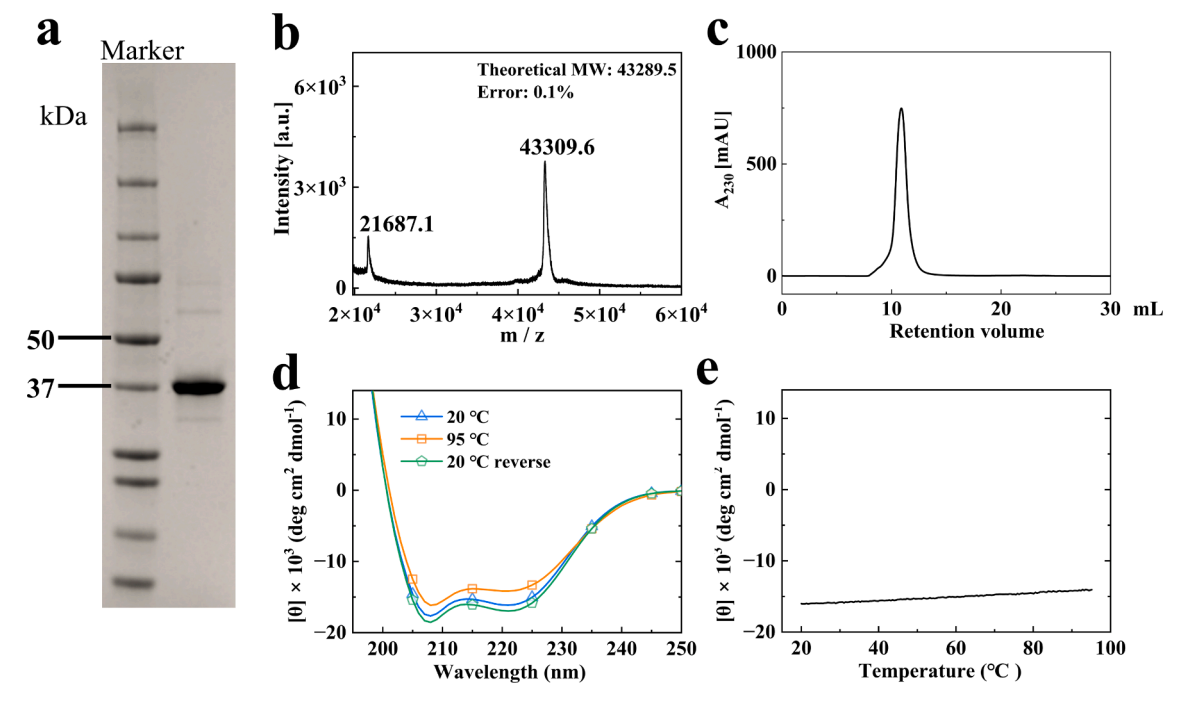


Fig. 2. Purification and characterization of PS-binding $\it B-M-E$ protein. a) SDS-PAGE analysis of the purified protein. Left, marker; right, protein after SEC purification. b) MALDI-TOF data. The two peaks in the MALDI-TOF spectra represent (protein + 2H)²⁺ and (protein + H)⁺. (c) Analytical SEC analysis. Absorbance at 230 nm as a function of retention volume. The peak at \sim 11 mL roughly corresponds to an Mw of 130 kDa, as expected for a $\it B-M-E$ trimer. (d) CD spectra showing mean residue molar ellipticity [θ] \times 10³ (deg cm² dmol⁻¹) as a function of wavelength. Blue line with triangles is the initial spectrum at 20 °C; orange line with squares represents the spectrum at 95 °C; and green line with pentagons indicates the spectrum cooling back to 20 °C. (e) Mean residue molar ellipticity at a wavelength of 220 nm plotted as a function of temperature with a heating ramp of 1 °C/min. Samples for all CD measurements were prepared at a concentration of 0.1 mg/mL in Milli-Q water.

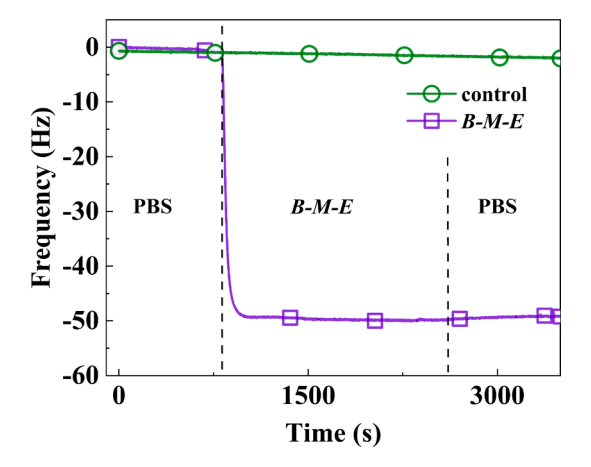


Fig. 3. QCM-D measurements indicate layer formation of PS-binding $\emph{B-M-E}$ proteins on PS coated quartz sensors. Frequency (Hz) shift versus time (s). The green line with circles represents a reference channel (only PBS); the purple line with squares is a sample channel (coated with $\emph{B-M-E}$ proteins). Samples for QCM-D were prepared at a concentration of 5 μ M in PBS, and all measurements were conducted at a flow rate of 50 μ L/min.

accurately estimate the adsorbed mass using the Sauerbrey equation [46]. Instead of applying more complicated models to account for the dissipation data, we simply use the frequency shift as a qualitative measure for the adsorbed mass.

To assess the homogeneity of the *B-M-E* protein layer on the PS surface, we performed AFM imaging (Fig. 4) on PS-coated quartz sensors (same sensors as for QCM), coated with *B-M-E* and subsequently dried. Micrographs of bare PS surfaces are shown in Fig. 4a and b, while PS surfaces coated with *B-M-E* are depicted in Fig. 4c and d. The PS-binding

B-M-E proteins uniformly covered the PS surface, consistent with previous findings for silica and gold surfaces coated with other version of **B-M-E** proteins [32,34].

Next, we used PS-nanoparticles (PS-NPs) with a hydrodynamic diameter (d) of 104.8 nm (standard deviation 0.7 nm; N = 3) to estimate the thickness (h) of the adsorbed B-M-E layers. The adsorbed B-M-E protein layers thickness was determined by measuring hydrodynamic diameter of PS-NPs before and after exposure to various concentrations of **B-M-E** using dynamic light scattering (DLS). PS-NPs were diluted 100 times from the stock concentration prior to mixing with the B-M-E proteins. B-M-E proteins were also diluted to a series of different concentrations: 0.01 $\mu M,\,0.1\,\mu M,\,1\,\mu M,\,5\,\mu M$ and 10 $\mu M.$ The grey sphere in Fig. 5a represents PS-NPs, while the blue and purple structure denotes the **B-M-E** proteins. Fig. 5b and c show the hydrodynamic diameters (D) of the coated particles and zeta potentials (ζ), respectively. In Fig. 5b, even at the lowest concentration of $\emph{B-M-E}$ proteins (0.01 μ M) used in this study, the hydrodynamic diameter (D) of the coated particles diameter of 139.0 nm (standard deviation 1.7 nm; N = 3) is already significantly larger than the diameter (d) of the bare PS-NPs. As shown in Fig. 5c, zeta potential was found to decrease from -5 mV for the bare PS-NPs to -34.0 mV for the **B-M-E** coated PS-NPs confirming the adsorption of B-M-E protein on PS-NPs. In the presence of excess B-M-E (10 μ M), the diameter of PS-NPs was estimated to be: 144.9 nm (standard deviation 1.9 nm; N = 3), as illustrated in Fig. 5a. From this value, we estimate a coating thickness (h) of approximately 20 nm using the formula h = (D - d)/2, where the diameter changes before and after protein coating on PS-NPs were evaluated. This should only be treated as a crude estimate, as measured small increase in thickness is quite sensitive to other effects, such as protein conformation or minor protein aggregation. However, this size increase is large enough to suggest the presence of a significant coating layer. Further details of the DLS data for mixtures of the PS-NPs and the B-M-E proteins, including an analysis of size

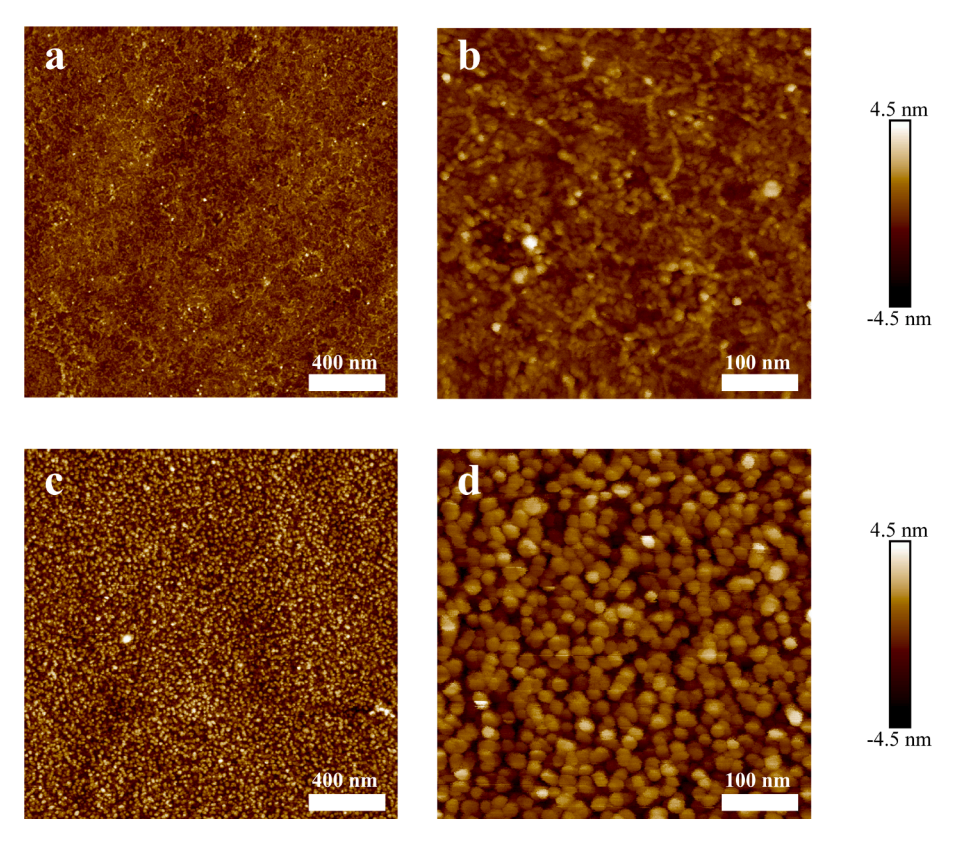


Fig. 4. Atomic force micrographs of bare PS surface and PS surface coated with *B-M-E* proteins. (a) Bare PS surface, $2 \mu m \times 2 \mu m$; (b) Enlarged micrograph of bare PS surface, $500 nm \times 500 nm$; (c) PS surface coated with $5 \mu M$ *B-M-E* for 5 min, $2 \mu m \times 2 \mu m$; (d) Enlarged micrograph of PS surface coated with $5 \mu M$ *B-M-E* for 5 min, $500 nm \times 500 nm$. All AFM measurements were performed in air.

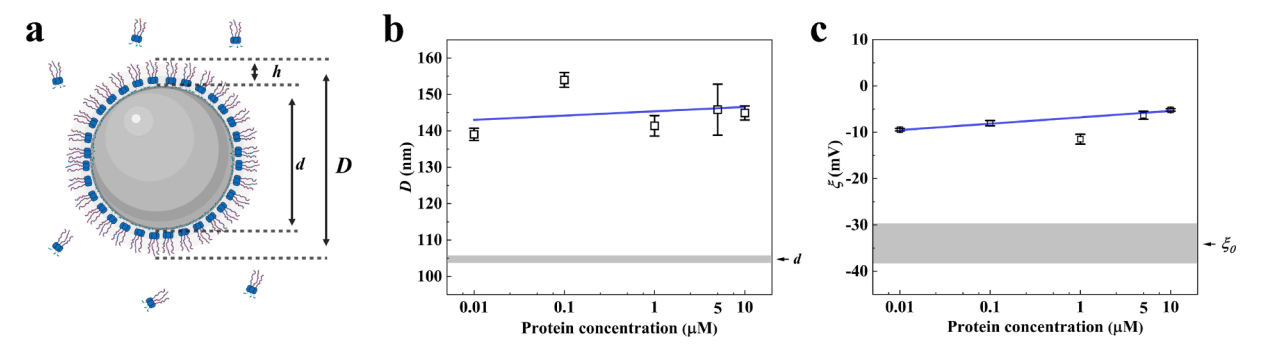


Fig. 5. DLS size and zeta potentials (ζ) results for mixtures of PS-NPs with a hydrodynamic diameter (d) of 104.8 nm (standard deviation 0.7 nm) and B-M-E proteins. a) Schematic illustration of adding excess B-M-E proteins to PS-NPs. b) Hydrodynamic diameter D (nm) of coated PS-NPs as a function of the concentration of B-M-E. The hydrodynamic diameter (d) of the PS-NPs with standard deviation is indicated by the gray bar. c) Zeta potential ζ (mV) of PS-NPs coated with B-M-E proteins, as a function of concentration. Initial zeta potential (ζ_0) value of the bare PS-NPs with standard deviation is indicated by the gray bar. The fitted value for both size and zeta potential measurements are shown in blue line. N = 3.

distributions resulting from the experiments, are given in Fig. S2.

A key feature for the adsorbed **B-M-E** proteins is the area occupied by the solid-binding peptides on the PS surface. Knowledge of this area would help determine whether densely packed B-M-E proteins on PS surfaces left any bare PS exposed or if the entire PS surface was fully covered by adsorbed B domains. To estimate the surface area occupied by the solid-binding peptide, we performed molecular dynamic (MD) simulations of a single PS-binding peptide adhering to a PS surface, using the AMBER forcefield for the peptide and aqueous solvent, and the GAFF forcefield for the PS. GAFF atom types and atomic charges for STO, STY and STN PS residues used in MD simulations are shown in Table S4. Definition of PS residues used in MD simulations are shown in Fig. S3. Exploring the various possible adsorbed conformations of solid-binding peptides on surfaces is challenging. Each transition requires releasing an existing set of contacts, adopting a new peptide conformation, and then forming a new set of contacts with the surface. This process typically has a large energy barrier [47]. To address the sampling problem, we used the simplest approximation. To obtain representative adsorbed configuration, we conducted multiple runs, each starting with the PS-binding peptide in solution. Five independently equilibrated configurations of the peptide in the simulation box were obtained (non-adsorbed). For each of these configurations, 150 ns MD simulations were performed in the presence of a PS surface. The peptide typically absorbed to the PS surface quickly, within the first few nanoseconds.

Two observables were calculated from the MD simulation trajectories. First, we determined the solvent-accessible surface area buried by each amino acid during adsorption process. We anticipate this information should help identify the residues that contribute most to surface anchoring. Second, we calculated the average projected area on the PS surface occupied by the adsorbed peptides. Results for the buried surface area per residue are shown in Fig. 6. The sequence of the PS-binding peptide we use here, VHWDFRQWWQPS, includes four strongly hydrophobic amino acids that could potentially act as anchors to the PS: Trp3, Phe5 and Trp8, Trp9. Fig. 6 clearly shows that Trp8 and Trp9, in particular, act as surface anchors. Surprisingly, the buried surface area of Trp3 was very small across all adsorbed configurations in our simulations, suggesting a limited contribution to binding. A movie of a typical trajectory for an adsorbed peptide shows more clearly that the Trp3 remains mobile and non-adsorbed (SI – movie 1).

Fig. 7a shows a typical adsorbed configuration of the PS-binding peptide on the PS surface. The Phe5, Trp8 and Trp9 have their aromatic rings inserted in between the styrene monomers, typically oriented perpendicular rather than parallel to the PS surface. However, we should caution about drawing too strong conclusions from these results, since the number of runs that we performed is still relatively small and hence sampling is limited. Fig. 7b. shows a top view space-filling representation of the peptide adsorbed to PS surface. On overage, the

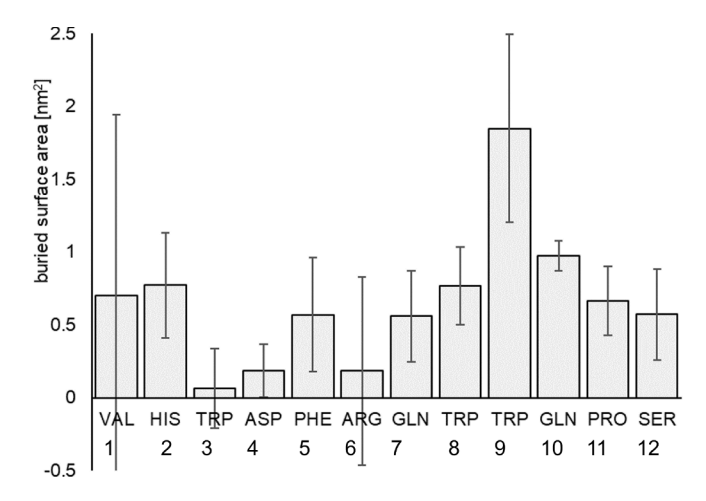


Fig. 6. Buried solvent accessible surface area upon peptide adsorption to PS for each amino acid in the sequence of the PS-binding peptide (VHWDFROWWOPS).

projected area occupied by the adsorbed peptide is approximately 1.5 nm², equivalent to a circular area with a cross-section of 1.4 nm. Fig. 7c shows the *M* block, with its N-terminus (to which the surface anchoring blocks *B* are connected) pointing downwards to a hypothetical PS-surface. At the N-termini, we have drawn circles with cross-sections of 1.4 nm. These data illustrate that even for the densely packed *B-M-E* coatings, the binding peptides would occupy only a small fraction of the total PS area. This implies that a significant part of the PS-surface remains uncovered by the binding peptides.

We emphasize that these MD simulations are preliminary in the sense that, for example, to properly sample the many adsorbed configurations. One would need to use sampling schemes such as replica exchange, that have been applied earlier to the cases of quartz-binding and gold-binding peptides [48,49]. However, using such more advanced schemes would not affect our conclusion that the PS-binding peptides cover only a part of the total PS area, even for dense brushes of the *B-M-E* proteins. Even more challenging would be to evaluate the free energy of adsorption for the solid-binding peptides from MD simulations. Owing to these challenges, among others, a recent computational study utilized novel deep learning techniques in conjunction with MD simulations to facilitate the molecular design of enhanced PS-binding peptide sequences [50].

2.3. Antifouling functionality

Next, we used a PS microfluidic channel device and QCM-D to

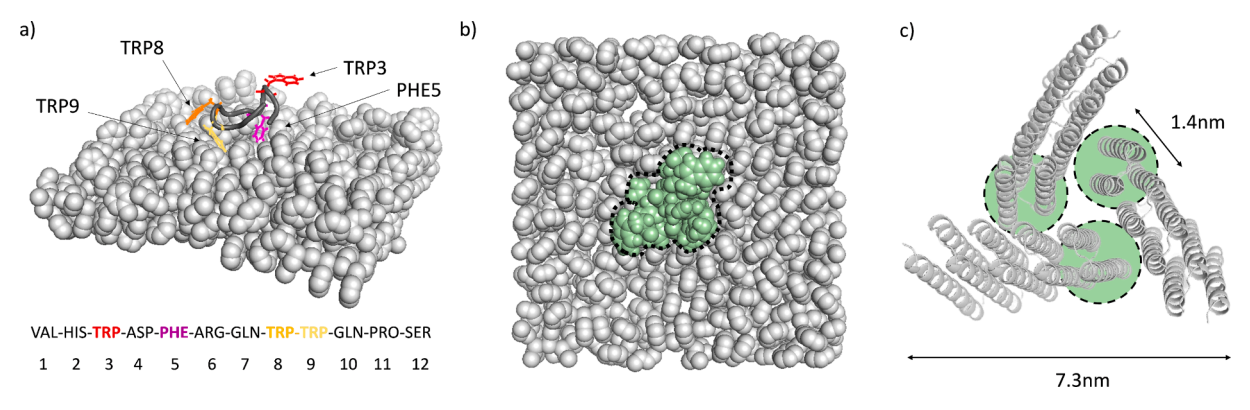


Fig. 7. MD simulation data. a) Conformation of PS-binding peptides on PS surface. Hydrophobic amino acid side chains for Trp3, Phe5 and Trp8, Trp9 are highlighted by colored bonds (red, purple, orange, and yellow, respectively). b) Top view of PS-binding peptide (green, space-filling) on PS surface (grey, space-filling). Projected surface area covered by PS-binding peptide indicated by black dotted line. The average projected surface area for all runs is approximately 1.5 nm². c) Average projected area of the PS-binding peptides, represented as circle with diameter 1.4 nm (green) below the N-termini of a trimer of the **M** block.

evaluate the antifouling activity of the PS-binding B-M-E proteins in preventing the nonspecific adsorption of BSA and human serum (HS). For the PS microfluidic channel assay, we compare two cases: a PS microfluidic channel that has been coated by B-M-E proteins (by flushing B-M-E into the channel, followed by rinsing with PBS) and an uncoated PS microfluidic channel as the control. As a fluorescent probe for fouling by proteins we use fluorescein isothiocyanate-labeled bovine serum albumin (FITC-BSA). A fouling step was performed by flushing FITC-BSA through the channels for a fixed duration, followed by rinsing with PBS to remove loosely bound FITC-BSA. Fig. 8a and b show fluorescence images of the uncoated reference and coated channels after the fouling step. The fluorescence intensity from FITC-BSA reflects the level of BSA adsorption on the surface, and thus the degree of fouling. Notably, the fluorescence intensity of the coated channel is significantly lower than that of the uncoated reference channel. These data clearly demonstrate that the B-M-E coating effectively inhibits the binding of FITC-BSA to the PS surface of the microchannels.

The images of the channels were analyzed to obtain the normalized fluorescence intensity along the white dashed lines indicated in Fig. 8a and b. The orange dotted line in Fig. 8a and b indicate the edges of the channels. The intensity traces shown in Fig. 8c again demonstrate that fluorescence (and thus fouling by FITC-BSA) is significantly lower in the coated microchannel compared to the uncoated one.

For a more rigorous and sensitive testing of fouling, we utilized QCM-D with increasing concentration of HS as a foulant. In Fig. 9a and b, the

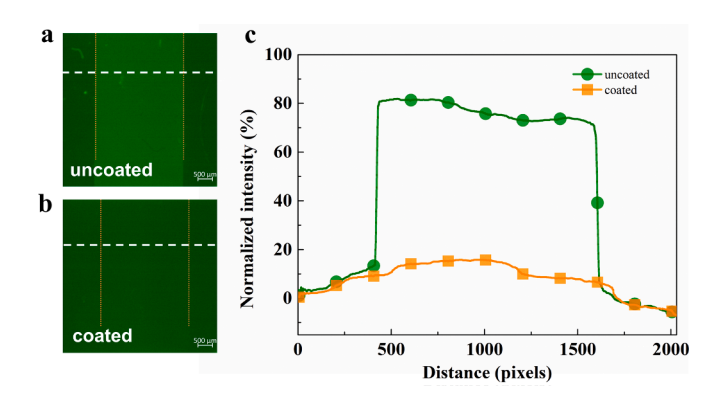


Fig. 8. Fouling on PS-microfluidic channels by flushing with 1 mg/mL FTIC-BSA for 30 min. Fluorescence micrograph of a) uncoated reference microfluidic channel, b) microfluidic channel coated with **B-M-E** proteins after the fouling step and final PBS flushing step. c) Normalized fluorescence intensity along the white dashed traces in panel a) and b). The green line with circles refers to the uncoated channel, while the orange line with squares represents the PS channel coated with **B-M-E** proteins.

initial decrease in frequency of the QCM-D sensor after injecting *B-M-E* protein indicates that the *B-M-E* proteins rapidly bind to the PS surface and reach saturation adsorption. Next, we observed some desorption in the following PBS flushing step (Fig. 9b). For confirmation of the stability of the *B-M-E* coating against prolonged PBS flushing, see Fig. S4.

After coating formation and PBS rinsing, we challenged the coatings by injecting HS. In Fig. 9 shows significant irreversible fouling for 1 % (v/v) HS and 10 % (v/v) HS for the uncoated PS. Frequency shifts between the timepoint just before the foulant injection and the timepoint at the end of the final flush with PBS was taken as a measure of fouling. These frequency changes were -38.8 Hz and -32.3 Hz for 1 % (v/v) HS and 10 % (v/v) HS on uncoated PS, respectively. In contrast, the corresponding frequency changes for the PS surfaces coated with $\textbf{\textit{B-M-E}}$ proteins were within experiment margin of error, with values of -0.6 Hz and -1.3 Hz for 1 % (v/v) HS and 10 % (v/v) HS, respectively. For completeness, representative QCM-D with dissipation data of $\textbf{\textit{B-M-E}}$ proteins against 1 % (v/v) HS and 10 % (v/v) HS are shown in Fig. S5.

We note that for the 10 % (v/v) HS experiments, there is an initial overshoot during the coating formation step. This phenomenon may be attributed to the self-association of B-M-E proteins in this case, resulting in the initial adsorption of larger B-M-E protein clusters, which were subsequently replaced by a more well-defined monolayer. Also, for the 10% (v/v) HS experiments, the frequency seems to show a small upward trend during the final PBS washing phase, possibly indicating either some desorption or some baseline instability. Based on the QCM-D results, we conclude that, to a good approximation, the coatings were stable against flushing with PBS, 1% (v/v) HS and 10% (v/v) HS.

Exposing the coating to more aggressive foulants, such as higher concentrations of HS, or using more sensitive techniques to measure foulant adsorption, would likely reveal the limitations in the stability and antifouling activity of the *B-M-E* coatings. In the following, we report on some improvements to the present PS-binding *B-M-E* design.

One potential direction for improvement is to replace the current PS-binding peptide sequence with a sequence with a higher surface-binding affinity. Although plenty of PS-binding peptide sequences have been reported [25,51,52], there is unfortunately limited comparative data on the binding affinity of different peptides on PS surfaces. Until such data become available, a practical approach might involve screening the antifouling performance of the B-M-E coating on PS surfaces against 10 % (v/v) HS or evaluating which PS-binding B blocks from a peptide library perform best. Considering the PS-binding peptide sequence we tested here, our MD simulation results suggest that one of the hydrophobic residues was mostly unable to bind to the PS surface, which is clearly suboptimal.

Another potential route towards stronger attachment is to increase the valency of the coating protein. This can be achieved in two ways. First, there are still a lot of uncovered PS surfaces even with densely

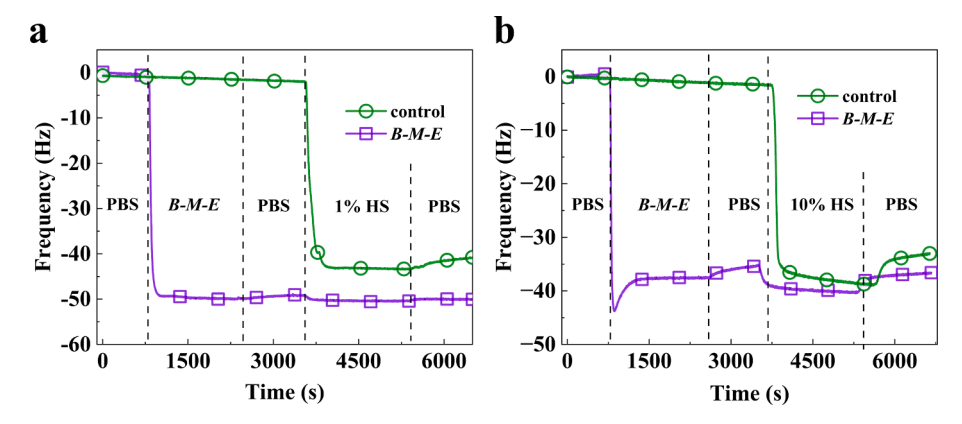


Fig. 9. QCM-D assay for testing the antifouling performance of *B-M-E* proteins on a PS surface. Firstly, a flat baseline was obtained by flushing QCM-D channel with PBS. Then, 5 μM *B-M-E* protein was injected for 30 min (PBS was injected in reference channel). After that, PBS was injected again for 15 min to flush off weakly bound proteins. Next, the foulant was injected for 30 min. Finally, we switch back to rinse surface with PBS. a) Foulant is 1 % (v/v) HS. b) Foulant is 10 % (v/v) HS.

packed B-M-E coatings. To address this issue, longer binding block B sequences, such as multiple repeats of PS-binding motifs, could be employed to cover a larger area on PS surfaces. Previous studies have demonstrated that a threefold tandem repeat of a gold-binding peptide exhibited a 5-fold increase in binding affinity and a 2.6-fold enhancement in surface coverage at room temperature on gold surfaces [53,54]. Second, the surface binding strength can also be improved by increasing the valency of the M domain. Employing new M with higher valency might modulate the adsorption induced rearrangements [55] then potentially lead to better surface packing density and better antifouling performance. Previously, we have found that while there is good modularity with respect to changing the **B** and **E** blocks [34], the choice of M is strongly limited by the practical requirements for good expression and solubility in E. coli [32]. Given the recent methodological developments in computational protein design [56–58], designing soluble, stable cyclic oligomers with control over N-terminal and C-terminal positioning is now much easier and we believe that an extension to higher valencies is achievable.

3. Concluding remarks

In this study, we combined experimental techniques with simulations to design a multiblock *B-M-E* protein to coat a PS surface. The *B-M-E* consists of *B*, PS-binding peptides for surface recognition; *M*, multimerization for overall binding strength and *E*, elastin-like polypeptides for antifouling functionality. We found that the *B-M-E* proteins effectively provide antifouling properties to PS surfaces through a simple one-step coating process. We confirmed that the *B-M-E* proteins formed homogenous brush layers on PS surfaces with good antifouling performance.

Stronger adhesion of the coating proteins to PS surfaces could possibly be achieved by employing PS-binding peptides with optimized affinity, by using longer tandem repeats of PS-binding peptides, or by increasing the valency of the *M* block. However, directly measuring the adhesion strength of the *B-M-E* proteins in the context of the fully formed coatings is difficult, since this strength is determined not only by the binding constant of single PS-binding peptides to the PS surface, but also by in-plane interactions between different PS-binding peptides, as we have established before for the case of silica-binding peptides [59]. To assess adhesion strength in screening designs, one can use strong displacers like surfactants and determine the critical displacer concentration required for coating detachment from the surface, as measured by QCM. After screening improved designs in these ways, we anticipate achieving effective antifouling performance, ease of application, and strong adhesion of the *B-M-E* coating proteins to PS surfaces.

4. Experimental section

4.1. Construction of expression plasmids

Primers, DNA sequences and amino acid sequences used in this study are correspondingly shown in Tables S1-3. PS-binding antifouling protein used in this study was reconstructed based on a previous goldbinding antifouling polypeptides design: H_6 - B^{GBP1} - E_3^S -M-E within pET-24(+) vector [34], where H_6 denotes six repeats of histidine as a purification tag, B^{GBP1} denotes a gold-binding peptide, E_3^S denotes elastinlike polypeptides with three repeat of GXGVP (single letter amino acid, X = S) motifs, M denotes a thermostable trimer previously de novo designed and characterized by Fallas et. al. [33], and E denotes elastinlike polypeptides with twenty repeats of (GXGVP, X = D/K) motifs. Based on the earlier H_6 - B^{GBP1} - E_3^S -M-E construct, Q5 polymer chain reaction was used to obtain linearized vector. A PS-binding peptide with a sequence of VHWDFRQWWQPS, was used here to replace the original gold-binding peptide. A gene fragment encoding PS-binding peptide with suitable overhangs for Gibson assembly [60] was purchased from Integrated DNA Technologies (IDT, Leuven, Belgium). Gibson assembly was used to insert gene fragment encoding PS-binding peptide into the linearized plasmid for H_6 - B^{GBP1} - E_3^S -M-E, yielding an expression plasmid for H_6 -B- E_3 -M-E. For brevity, we will use B-M-E abbreviation to represent the H_6 -B- E_3^S -M-E, unless otherwise specified.

4.2. Protein expression and protein purification

All plasmids used in this study were sequenced before starting protein expression. Plasmids containing the desired DNA sequences were transformed into T7-Express E. coli (New England Biolabs, USA). The transformed strains were cultured in 25 mL of Terrific Broth medium containing 50 µg/mL kanamycin in 250 mL Erlenmeyer flasks at 37 °C with shaking at 215 rpm for at least 16 h to prepare the starting culture. The starter culture was diluted in 1 L autoclaved Lysogeny Broth medium (tryptone 10 g/L, NaCl 10 g/L, yeast extract 5 g/L, 50 µg/mL kanamycin). Isopropylthio-β-galactoside was added to the Lysogeny Broth medium at a final concentration of 1 mM when the culture optical density at 600 nm reached a range from 0.6 to 0.8. Next, bacteria were incubated for more than 21 h at 18 °C with shaking at 215 rpm. After overnight protein expression, cultures were centrifuged at 6000 rpm at 4 °C for 30 min to pellet the cells. Bacterial pellets were resuspended in 30 mL of cold lysis buffer (50 mM Tris pH 8.00, 300 mM NaCl, 30 mM imidazole). Then, 300 μL of 0.1 M phenylmethylsulfonyl fluoride was added to lysis buffer containing bacteria to a final concentration of $\boldsymbol{1}$ mM. Next, resuspended cells were sonicated using a Q125 Sonicator (Qsonica) with a 2-s on/off duty cycle at 85 % amplitude for 7 min. After sonication, the bacterial lysate was centrifuged at centrifuged at 13,000

rpm at 4 °C for 30 min to obtain supernatant with soluble overexpressed proteins. Overexpressed proteins were isolated from the supernatant using a 25 mL gravity immobilized metal ion affinity chromatography column (Bio-Scale Mini Profinity IMAC cartridge, Bio-Rad Laboratories, USA). Then, the column was washed with 50 mL lysis buffer after protein bound to column. A 6-mL aliquot of elution buffer (50 mM Tris pH 8.00, 300 mM NaCl, 300 mM imidazole) was used to elute protein. Eluted proteins were filtered using a 0.22 µm filter (Millex®-GV, Sigma) and then purified by size exclusion chromatography (SEC) with using Superdex 200 Increase 10/300GL column (GE Healthcare). *SEC* purification was performed at a flow rate of 0.75 mL/min in phosphate-buffered saline (PBS) pH 7.4 on a 1260 infinity II HPLC (Agilent). Purity of the proteins throughout the purification process was monitored using sodium dodecyl-sulfate poly(acrylamide) gel electrophoresis (SDS-PAGE).

4.3. Matrix assisted laser desorption/ionization-time of flight (MALDI-TOF) mass spectrometry

Mass spectra of *B-M-E* proteins were obtained using a Bruker UltraFlextreme spectrometer (Bruker Daltonics). Samples were dialyzed in Milli-Q water using Slide-A-Lyzer MINI Dialysis Device with 3.5 kDa cut off (Thermo Scientific) prior to measurement. Then, the dialyzed protein samples were concentrated to 1 mg/mL. Next, matrix solutions for measurement were prepared as follows: 5 mg 2,5-Dihydroxybenzoic acid were dissolved in 200 μ L Milli-Q water/0.1 % formic acid in acetonitrile (v/v). Then, 1 μ L matrix was placed on a target plate (MTP 384 target plate ground steel T F, Bruker), followed by 1 μ L of protein solution. After that, the mixed samples were gently dried using a hair dryer. Data were processed using Bruker FlexAnalysis version 3.4.

4.4. Circular dichroism (CD)

A Jasco Spectropolarimeter J-715 was used to measure CD spectra. Samples were dialyzed in Milli-Q water using Slide-A-Lyzer MINI Dialysis Device with 3.5 kDa cut off (Thermo Scientific) prior to measurement. All samples were diluted to 0.1 mg/mL (in PBS) and placed into a sonication bath for 10 min to minimize potential aggregation prior to CD measurements. All measurements were performed in a quartz cuvette (QS 110-1-40, Hellma Analytics) with a 1 mm path. For spectra, a continuous scanning mode with a wavelength step size of 0.1 nm and a band width of 2 nm was used. The spectra represent the average of 15 individually acquired spectra. For temperature ramp measurements, the mean residue molar ellipticity at 220 nm was continuously monitored from 20 °C to 95 °C at a heating rate of 1 °C/min.

4.5. Quartz crystal microbalance with dissipation (QCM-D)

Both PS-coated quartz sensors (QS-QSX305) and Q-Sense E4 QCM-D instrument were purchased from Biolin Scientific (Sweden). *B-M-E* protein solutions were diluted to 5 μ M in PBS, filtered through a 0.22 μ m pore size filter, and sonicated for 5 min prior to measurements. For QCM measurements, both protein coating formation and antifouling test were performed at a flow rate of 50 μ L/min. First, a flat QCM-D base line was obtained by prolonged (at least 10 min) PBS flushing. This was done until frequency variations were less than ~2 Hz. Next, *B-M-E* proteins were immobilized on each sensor for 30 min, followed by a 15-min PBS wash step. Finally, 1 % (v/v) or 10 % (v/v) HS was injected into the QCM-D channels to analyze the antifouling behavior of the coating, followed by a 15-min PBS wash step. The QCM-D data were analyzed using the QSense Dfind version 1.2.7 (Biolin Scientific, Sweden).

4.6. Atomic force microscopy (AFM)

PS coated quartz sensors (QS-QSX305, Biolin Scientific, Sweden) were used as the AFM substrate. PS surfaces were first cleaned by

extensively rinsing with Milli-Q water and then dried using nitrogen gas. To prepare samples for AFM imaging, A 50 μL aliquot of 5 μL $\emph{B-M-E}$ protein solution (in PBS) was placed on a PS surface 5 min at room temperature. After incubation, samples were again rinsed with Milli-Q water and dried using nitrogen gas. Next, the PS sensors were imaged using a Multimode AFM (Bruker, California) with the ScanAsyst imaging mode in air. ScanAsyst Air cantilevers (Bruker, California) were used with the following specifications: thickness 650 nm, length 115 μm , width 25 μm , resonance frequency 70 kHz, spring constant 0.4 N/m. Data were analyzed by NanoScope Analysis version 1.5 (Bruker, California).

4.7. Molecular dynamics (MD) simulations

MD simulations were carried out using OpenMM [61], running on NVIDIA V100 GPU processors. For the biomolecular parts of the system, we use the AMBER forcefield, in combination with TIP3P for the water and ions. For the PS polymers, we use the General Amber Force Field (GAFF), developed to parametrize arbitrary molecules interacting with (hydrated) biomolecules [62]. OpenMM defines molecules in terms of residues. We chose to model PS molecules in terms of STO and STN "terminal" residues and STY "internal" residues, as defined in Fig. S3b-d. Next to the fixed parameter of the GAFF forcefield, a complete parametrization then also requires atomic partial charges for atoms in the STO, STN and STY residues. To obtain these, we used the AM1-BCC method [63], as implemented in AmberTools [64], to calculate partial atomic charges for atoms in an isotactic (styrene)₄ oligomer (Fig. S3a). Coordinates for the isotactic (styrene)₄ oligomer were obtained by manually drawing the isotactic (styrene)₄ oligomer in Chem3D software. Next, within the Chem3D software a MM minimization was performed using the GAFF forcefield. Values of atomic charges for the atoms in the STO, STY and STN residues obtained from the AM1-BCC calculation are given in Table S4. Forcefield files for AMBER and GAFF are included with OpenMM. To run the PS simulations, we included a single extra forcefield file that defines the topology of the PS residues and gives the values of the atomic charges. This file was provided in the Supplementary Information.

Models for atactic (styrene) $_{50}$ molecules were constructed by joining together models for isotactic (styrene) $_4$ oligomers (and removing monomers as required), using RDKit for Python. To generate quenched PS slabs, identical atactic PS molecules were first equilibrated (in vacuum) in a cubic simulation box with periodic boundary conditions, through Molecular Dynamics simulation runs at a high temperature. After these runs, PS polymers spread randomly throughout the simulation box. Next, an external potential was used to compress the polymers to a slab in the xy-directions, again through MD simulation runs at high temperature. The model for the PS-slab was combined with a model for the PS-binding peptide VHWDFRQWWQPS (in an extended configuration) and OpenMM was used to solvate the combined system using TIP3P water molecules.

The solvated system was first equilibrated through NPT MD, using the OpenMM "LangevinMiddleIntegrator" with a friction constant of 1.0 ps $^{-1}$, at a temperature of T = 298 K, and a stepsize of 2 fs. A constant pressure of 1.0 bar was maintained by using the OpenMM "monteCarloAnisotropicBarostat", allowing the boxsize to only change in the *z*-direction, thus maintaining the structure of the PS slab in the *xy*-plane. The NPT equilibration runs were 20 ns long. After the NPT run, the dimensions of the cubic simulation box in the *x*,*y* and *z* directions were, respectively, 6.0, 6.0 and 5.4 nm.

Next, a longer NVT Molecular Dynamics equilibration run was performed, again using the OpenMM "LangevinMiddleIntegrator" with a friction constant of $1.0~{\rm ps}^{-1}$, at a temperature of $T=298~{\rm K}$, and a stepsize of 2 fs. The overall shape of PS slab was maintained by fixing the "CA" atom of the styrene residues, by giving these a large mass. Similarly, PS-binding peptide was prevented from diffusing to and adsorbing on the surface by fixing the "CA" atom of its ARG residue (located in the

middle of the sequence). This NVT equilibration run was 120 ns long, the 5 configurations at t=20, 40, 60, 80, 100 and 120 ns were used as independent starting points for the subsequent production runs in which the peptides were allowed to absorb to the PS surface.

For each of the 5 initial configurations, NVT Molecular Dynamics production runs were performed, again using the "LangevinMiddleIntegrator" with a friction constant of $1.0~\rm ps^{-1}$, at a temperature of $T=298~\rm K$, and a stepsize of 2 fs. Again, the overall shape of PS slab was maintained by fixing the "CA" atom of the styrene residues, by giving these a large mass, but for the production runs the peptides were free to adsorb to the PS surface. Each production run was $100~\rm ns$ long. In each case adsorption of the peptide to the PS surface was rapid, within the first a few nanoseconds. From the molecular trajectories of the production runs, the solvent-accessible surface area buried upon adsorption, and the area of the adsorbed peptides projected on the xy-plane were calculated using MDtraj [65]. The spread over the 5 runs was used as an estimate of the error in determining the average per-residue buried solvent-accessible surface area and the area on the xy-plane occupied by the adsorbed peptides.

4.8. Dynamic light scattering (DLS)

A ZS-Nano instrument (Malvern, UK) with scattering angle of 173° was used to measure the hydrodynamic size of PS nanoparticles before and after protein coating. Protein samples were filtered using a 0.22 μm pore size filter then diluted in PBS to a series of concentrations: 0.01 μM , 0.1 μM , 1 μM , 5 μM and 10 μM . Then samples were placed into a sonication water bath for 5 min prior to use. All protein size measurements were performed in a quartz cuvette (105.251.005-QS, Hellma Analytics) with a light path of 3 mm at 20 °C. Each reported particle size represents the average value of 15 independent measurements. DLS data were analyzed by Zetasizer software version 7.13 (Malvern, U.K.).

4.9. Microfluidic channel measurement

PS microfluidic chips were purchased from microfluidic ChipShop (Germany). Images for antifouling experiments were acquired using a ZEISS microscope (Axio Observer 7) equipped with Light Source Colibri 5 (Type RGB-UV) and a ZEISS Plan-NEOFLUAR 2.5x/0.5 objective. For fluorescence visualization, samples were excited with 20 % of the maximum intensity and images were acquired at exposure of 100 ms, using a Prime BSI Express sCMOS camera. For the measurement, two channels were incubated with PBS for 10 min. Subsequently, the test channel was treated with 5 μ M PS-binding **B-M-E** proteins for 30 min, while the reference channel was maintained with PBS. Both channels were then incubated with FITC-BSA (1 mg/mL) at a flow rate of 50 μ L/min for 30 min. Finally, both channels were flushed with PBS for 15 min to remove any unbound FITC-BSA. Fluorescent images of the channels were captured using identical microscope settings. Data were analyzed by ImageJ and Origin.

CRediT authorship contribution statement

Chuanbao Zheng: Writing – review & editing, Writing – original draft, Methodology, Investigation, Formal analysis, Data curation, Conceptualization. Zohaib Hussain: Formal analysis, Data curation. Chang Chen: Formal analysis, Data curation. Robbert Jan de Haas: Formal analysis, Data curation. Siddharth Deshpande: Writing – review & editing, Supervision. Zhisen Zhang: Writing – review & editing, Supervision. Han Zuilhof: Writing – review & editing, Supervision. Renko de Vries: Writing – review & editing, Writing – original draft, Validation, Supervision, Software, Project administration, Methodology, Investigation, Funding acquisition, Formal analysis, Data curation, Conceptualization.

Declaration of competing interest

The authors declare that they have no known competing financial interests or personal relationships that could have appeared to influence the work reported in this paper.

Acknowledgment

C.Z acknowledges a fellowship from the China Scholarship Council (No. 202006310052). R.J.d.H acknowledges a fellowship from VLAG Graduate School Research.

Appendix A. Supplementary data

Primers, DNA sequences, amino acid sequences, and additional DLS, simulation and QCM-D data are shown in supporting information. Representative simulation trajectory and simulation force field are shown in SI-movie1, and force filed file, respectively. Supplementary data to this article can be found online at https://doi.org/10.1016/j.jcis.2025.01.147.

Data availability

Data will be made available on request.

References

- G.P. Sakala, M. Reches, Peptide-based approaches to fight biofouling, Adv. Mater. Int. 5 (2018) 1800073, https://doi.org/10.1002/admi.201800073.
- [2] A.M.C. Maan, A.H. Hofman, W.M. de Vos, M. Kamperman, Recent developments and practical feasibility of polymer-based antifouling coatings, Adv. Funct. Mater. 30 (2020) 2000936, https://doi.org/10.1002/adfm.202000936.
- [3] R.E. Armstrong, M. Horáček, P. Zijlstra, Plasmonic assemblies for real-time single-molecule biosensing, Small 16 (2020) 2003934, https://doi.org/10.1002/smll.202003934.
- [4] J. Tian, Y. Liu, S. Miao, Q. Yang, X. Hu, Q. Han, L. Xue, P. Yang, Amyloid-like protein aggregates combining antifouling with antibacterial activity, Biomater. Sci. 8 (2020) 6903–6911, https://doi.org/10.1039/D0BM00760A.
- [5] A.T. Speidel, P.R.A. Chivers, C.S. Wood, D.A. Roberts, I.P. Correia, A.S. Caravaca, Y.K.V. Chan, C.S. Hansel, J. Heimgärtner, E. Müller, J. Ziesmer, G.A. Sotiriou, P. S. Olofsson, M.M. Stevens, Tailored biocompatible polyurethane-poly(ethylene glycol) hydrogels as a versatile nonfouling biomaterial, Adv. Healthc. Mater. 11 (2022) 2201378, https://doi.org/10.1002/adhm.202201378.
- [6] X. Song, J. Man, Y. Qiu, J. Wang, J. Liu, R. Li, Y. Zhang, J. Li, J. Li, Y. Chen, Design, preparation, and characterization of lubricating polymer brushes for biomedical applications, Acta Biomater. 175 (2024) 76–105, https://doi.org/10.1016/j.actbio.2023.12.024.
- [7] C.D. Flynn, D. Chang, A. Mahmud, H. Yousefi, J. Das, K.T. Riordan, E.H. Sargent, S. O. Kelley, Biomolecular sensors for advanced physiological monitoring, Nat. Rev. Bioeng. 1 (2023) 560–575, https://doi.org/10.1038/s44222-023-00067-z.
- [8] M. Charnley, M. Textor, C. Acikgoz, Designed polymer structures with antifouling-antimicrobial properties, React. Funct. Polym. 71 (2011) 329–334, https://doi.org/10.1016/j.reactfunctpolym.2010.10.013.
- [9] X. Hu, J. Tian, C. Li, H. Su, R. Qin, Y. Wang, X. Cao, P. Yang, Amyloid-like protein aggregates: a new class of bioinspired materials merging an interfacial anchor with antifouling, Adv. Mater. 32 (2020) 2000128, https://doi.org/10.1002/ adma.202000128.
- [10] I. Banerjee, R.C. Pangule, R.S. Kane, Antifouling coatings: recent developments in the design of surfaces that prevent fouling by proteins, bacteria, and marine organisms, Adv. Mater. 23 (2011) 690–718, https://doi.org/10.1002/ adma.201001215.
- [11] M. Garay-Sarmiento, L. Witzdam, M. Vorobii, C. Simons, N. Herrmann, A. de los Santos Pereira, E. Heine, I. El-Awaad, R. Lütticken, F. Jakob, U. Schwaneberg, C. Rodriguez-Emmenegger, Kill&Repel coatings: the marriage of antifouling and bactericidal properties to mitigate and treat wound infections, Adv. Funct. Mater. 32 (2022) 2106656, https://doi.org/10.1002/adfm.202106656.
- [12] X. Zang, Y. Ni, Q. Wang, Y. Cheng, J. Huang, X. Cao, C.J. Carmalt, Y. Lai, D. Ha Kim, Y. Liu, Z. Lin, Non-toxic evolution: Advances in multifunctional antifouling coatings, Mater. Today (2024), https://doi.org/10.1016/j.mattod.2024.03.018.
- [13] X. Xu, Y. Chang, Y. Gong, Y. Zhang, Y. Yu, H. Peng, C. Fu, Recent advances in antifouling surface polymer brushes, ACS Appl. Polym. Mater. 6 (2024) 1–27, https://doi.org/10.1021/acsapm.3c02150.
- [14] C. Fu, Z. Wang, X. Zhou, B. Hu, C. Li, P. Yang, Protein-based bioactive coatings: from nanoarchitectonics to applications, Chem. Soc. Rev. 53 (2024) 1514–1551, https://doi.org/10.1039/D3CS00786C.
- [15] S.C. Lange, E. van Andel, M.M.J. Smulders, H. Zuilhof, Efficient and tunable threedimensional functionalization of fully zwitterionic antifouling surface coatings,

- Langmuir 32 (2016) 10199–10205, https://doi.org/10.1021/acs.
- [16] A.R. Kuzmyn, A.T. Nguyen, L.W. Teunissen, H. Zuilhof, J. Baggerman, Antifouling polymer brushes via oxygen-tolerant surface-initiated PET-RAFT, Langmuir 36 (2020) 4439–4446, https://doi.org/10.1021/acs.langmuir.9b03536.
- [17] C.-M. Zhang, Y.-Z. Qiu, H. Wu, J. Guan, S.-G. Wang, X.-F. Sun, Polyethylene glycol-polyvinylidene fluoride/TiO2 nanocomposite polymer coatings with efficient antifouling strategies: Hydrophilized defensive surface and stable capacitive deionization, J. Colloid Interface Sci. 666 (2024) 585–593, https://doi.org/10.1016/j.jcis.2024.03.147.
- [18] S. Chen, Z. Cao, S. Jiang, Ultra-low fouling peptide surfaces derived from natural amino acids, Biomaterials 30 (2009) 5892–5896, https://doi.org/10.1016/j. biomaterials 2009 07 001
- [19] T. Riedel, Z. Riedelová-Reicheltová, P. Májek, C. Rodriguez-Emmenegger, M. Houska, J.E. Dyr, E. Brynda, Complete identification of proteins responsible for human blood plasma fouling on poly(ethylene glycol)-based surfaces, Langmuir 29 (2013) 3388–3397, https://doi.org/10.1021/la304886r.
- [20] L.W. Teunissen, A.R. Kuzmyn, F.S. Ruggeri, M.M.J. Smulders, H. Zuilhof, Thermoresponsive, pyrrolidone-based antifouling polymer brushes, advanced materials, Interfaces 9 (2022) 2101717, https://doi.org/10.1002/ admi.202101717.
- [21] A.R. Kuzmyn, L.W. Teunissen, P. Fritz, B. van Lagen, M.M.J. Smulders, H. Zuilhof, Diblock and random antifouling bioactive polymer brushes on gold surfaces by visible-light-induced polymerization (SI-PET-RAFT) in water, Adv. Mater. Interfaces 9 (2022) 2101784, https://doi.org/10.1002/admi.202101784.
- [22] J. Andersson, J. Järlebark, S. KK, A. Schaefer, R. Hailes, C. Palasingh, B. Santoso, V.-T. Vu, C.-J. Huang, F. Westerlund, A. Dahlin, Polymer brushes on silica nanostructures prepared by aminopropylsilatrane click chemistry: superior antifouling and biofunctionality, ACS Appl. Mater. Interfaces 15 (2023) 10228–10239, https://doi.org/10.1021/acsami_2c21168.
- [23] D. Di Iorio, S. Rameshbabu, B. Bruijns, J. Movilli, M. Skolimowski, J. Huskens, Click-and-bond: room-temperature and solvent-free bonding of polymer-based microfluidic devices, Adv. Mater. Interfaces 9 (2022) 2200282, https://doi.org/ 10.1002/admi.202200282.
- [24] N. Bellassai, A. Marti, G. Spoto, J. Huskens, Low-fouling, mixed-charge poly-1 -lysine polymers with anionic oligopeptide side-chains, J. Mater. Chem. B 6 (2018) 7662–7673, https://doi.org/10.1039/C8TB01619D.
- [25] N. Alvisi, R. de Vries, Biomedical applications of solid-binding peptides and proteins, Mater. Today Bio 19 (2023) 100580, https://doi.org/10.1016/j. mtbio.2023.100580.
- [26] S. Brown, Metal-recognition by repeating polypeptides, Nat. Biotechnol. 15 (1997) 269–272. https://doi.org/10.1038/nbt0397-269.
- [27] R. Hassert, M. Pagel, Z. Ming, T. Häupl, B. Abel, K. Braun, M. Wiessler, A.G. Beck-Sickinger, Biocompatible silicon surfaces through orthogonal click chemistries and a high affinity silicon oxide binding peptide, Bioconjugate Chem. 23 (2012) 2129–2137. https://doi.org/10.1021/bc3003875.
- [28] A. Care, P.L. Bergquist, A. Sunna, Solid-binding peptides: smart tools for nanobiotechnology, Trends Biotechnol. 33 (2015) 259–268, https://doi.org/ 10.1016/j.tibtech.2015.02.005.
- [29] S.R. MacEwan, A. Chilkoti, Elastin-like polypeptides: Biomedical applications of tunable biopolymers, Pept. Sci. 94 (2010) 60–77, https://doi.org/10.1002/ bip.21327.
- [30] A.K. Varanko, J.C. Su, A. Chilkoti, Elastin-like polypeptides for biomedical applications, Annu. Rev. Biomed. Eng. 22 (2020) 343–369, https://doi.org/ 10.1146/annurev-bioeng-092419-061127.
- [31] E. Garanger, S. Lecommandoux, Emerging opportunities in bioconjugates of Elastin-like polypeptides with synthetic or natural polymers, Adv. Drug Deliv. Rev. 191 (2022) 114589. https://doi.org/10.1016/j.addr.2022.114589.
- [32] N. Alvisi, C. Zheng, M. Lokker, V. Boekestein, R. de Haas, B. Albada, R. de Vries, Design of polypeptides self-assembling into antifouling coatings: exploiting multivalency, Biomacromolecules 23 (2022) 3507–3516, https://doi.org/ 10.1021/acs.biomacr2c0170
- [33] J.A. Fallas, G. Ueda, W. Sheffler, V. Nguyen, D.E. McNamara, B. Sankaran, J. H. Pereira, F. Parmeggiani, T.J. Brunette, D. Cascio, T.R. Yeates, P. Zwart, D. Baker, Computational design of self-assembling cyclic protein homo-oligomers, Nature Chem. 9 (2017) 353–360, https://doi.org/10.1038/nchem.2673.
- [34] C. Zheng, N. Alvisi, R.J. de Haas, Z. Zhang, H. Zuilhof, R. de Vries, Modular design for proteins assembling into antifouling coatings: case of gold surfaces, Langmuir (2023), https://doi.org/10.1021/acs.langmuir.3c00389.
- [35] L. Pinchuk, G.J. Wilson, J.J. Barry, R.T. Schoephoerster, J.-M. Parel, J.P. Kennedy, Medical applications of poly(styrene-block-isobutylene-block-styrene) ("SIBS"), Biomaterials 29 (2008) 448–460, https://doi.org/10.1016/j. biomaterials.2007.09.041.
- [36] C. Liao, M. Zhang, M.Y. Yao, T. Hua, L. Li, F. Yan, Flexible organic electronics in biology: materials and devices, Adv. Mater. 27 (2015) 7493–7527, https://doi.org/ 10.1002/adma.201402655
- [37] T. Someya, Z. Bao, G.G. Malliaras, The rise of plastic bioelectronics, Nature 540 (2016) 379–385, https://doi.org/10.1038/nature21004.
- [38] G.F. Meyers, B.M. DeKoven, J.T. Seitz, Is the molecular surface of polystyrene really glassy? Langmuir 8 (1992) 2330–2335, https://doi.org/10.1021/ 12000455042
- [39] G. Cheng, G. Li, H. Xue, S. Chen, J.D. Bryers, S. Jiang, Zwitterionic carboxybetaine polymer surfaces and their resistance to long-term biofilm formation, Biomaterials 30 (2009) 5234–5240, https://doi.org/10.1016/j.biomaterials.2009.05.058.
- [40] H.S. Sundaram, X. Han, A.K. Nowinski, J.-R. Ella-Menye, C. Wimbish, P. Marek, K. Senecal, S. Jiang, One-step dip coating of zwitterionic sulfobetaine polymers on

- hydrophobic and hydrophilic surfaces, ACS Appl. Mater. Interfaces 6 (2014) 6664–6671, https://doi.org/10.1021/am500362k.
- [41] A.M.C. Maan, C.N. Graafsma, A.H. Hofman, T. Pelras, W.M. de Vos, M. Kamperman, Scalable fabrication of reversible antifouling block copolymer coatings via adsorption strategies, ACS Appl. Mater. Interfaces 15 (2023) 19682–19694, https://doi.org/10.1021/acsami.3c01060.
- [42] Y. Kumada, Y. Shiritani, K. Hamasaki, T. Ohse, M. Kishimoto, High biological activity of a recombinant protein immobilized onto polystyrene, Biotechnol. J. 4 (2009) 1178–1189, https://doi.org/10.1002/biot.200800192.
- [43] S. Konagaya, K. Kato, T. Nakaji-Hirabayashi, H. Iwata, Design of culture substrates for large-scale expansion of neural stem cells, Biomaterials 32 (2011) 992–1001, https://doi.org/10.1016/ji.biomaterials.2010.10.008.
- [44] X. Qiang, K. Sun, L. Xing, Y. Xu, H. Wang, Z. Zhou, J. Zhang, F. Zhang, B. Caliskan, M. Wang, Z. Qiu, Discovery of a polystyrene binding peptide isolated from phage display library and its application in peptide immobilization, Sci. Rep. 7 (2017) 2673, https://doi.org/10.1038/s41598-017-02891-x.
- [45] W.C.J. Jr, Secondary structure of proteins through circular dichroism spectroscopy, Annu. Rev. Biophys. 17 (1988) 145–166, https://doi.org/10.1146/annurev. bb.17.060188.001045.
- [46] G. Sauerbrey, Verwendung von Schwingquarzen zur Wägung dünner Schichten und zur Mikrowägung, Z. Physik 155 (1959) 206–222, https://doi.org/10.1007/ BF01337937.
- [47] M. Mijajlovic, M.J. Penna, M.J. Biggs, Free energy of adsorption for a peptide at a liquid/solid interface via nonequilibrium molecular dynamics, Langmuir 29 (2013) 2919–2926, https://doi.org/10.1021/la3047966.
- [48] R. Notman, E.E. Oren, C. Tamerler, M. Sarikaya, R. Samudrala, T.R. Walsh, Solution study of engineered quartz binding peptides using replica exchange molecular dynamics, Biomacromolecules 11 (2010) 3266–3274, https://doi.org/ 10.1021/bm100646z.
- [49] S. Corni, M. Hnilova, C. Tamerler, M. Sarikaya, Conformational behavior of genetically-engineered dodecapeptides as a determinant of binding affinity for gold, J. Phys. Chem. C 117 (2013) 16990–17003, https://doi.org/10.1021/ ip404057h.
- [50] M.T. Bergman, X. Xiao, C.K. Hall, In silico design and analysis of plastic-binding peptides, J. Phys. Chem. B 127 (2023) 8370–8381, https://doi.org/10.1021/acs. jpcb.3c04319.
- [51] N. Li, J. Kang, L. Jiang, B. He, H. Lin, J. Huang, PSBinder: a web service for predicting polystyrene surface-binding peptides, Biomed Res. Int. 2017 (2017) 1–5, https://doi.org/10.1155/2017/5761517.
- [52] H. Woo, S. Hyun Kang, Y. Kwon, Y. Choi, J. Kim, D.-H. Ha, M. Tanaka, M. Okochi, J. Su Kim, H. Koo Kim, J. Choi, Sensitive and specific capture of polystyrene and polypropylene microplastics using engineered peptide biosensors, RSC Adv. 12 (2022) 7680–7688, https://doi.org/10.1039/D1RA08701K.
- [53] C. Tamerler, E.E. Oren, M. Duman, E. Venkatasubramanian, M. Sarikaya, Adsorption kinetics of an engineered gold binding peptide by surface plasmon resonance spectroscopy and a quartz crystal microbalance, Langmuir 22 (2006) 7712–7718, https://doi.org/10.1021/la0606897.
- [54] U.O.S. Seker, B. Wilson, J.L. Kulp, J.S. Evans, C. Tamerler, M. Sarikaya, Thermodynamics of engineered gold binding peptides: establishing the structure–activity relationships, Biomacromolecules 15 (2014) 2369–2377, https://doi.org/10.1021/bm4019006.
- [55] P. Roach, D. Farrar, C.C. Perry, Interpretation of protein adsorption: surfaceinduced conformational changes, J. Am. Chem. Soc. 127 (2005) 8168–8173, https://doi.org/10.1021/ja0428980.
- [56] J. Jumper, R. Evans, A. Pritzel, T. Green, M. Figurnov, O. Ronneberger, K. Tunyasuvunakool, R. Bates, A. Žídek, A. Potapenko, A. Bridgland, C. Meyer, S.A. A. Kohl, A.J. Ballard, A. Cowie, B. Romera-Paredes, S. Nikolov, R. Jain, J. Adler, T. Back, S. Petersen, D. Reiman, E. Clancy, M. Zielinski, M. Steinegger, M. Pacholska, T. Berghammer, S. Bodenstein, D. Silver, O. Vinyals, A.W. Senior, K. Kavukcuoglu, P. Kohli, D. Hassabis, Highly accurate protein structure prediction with AlphaFold, Nature 596 (2021) 583–589, https://doi.org/10.1038/s41586-021_03819-2
- [57] J. Dauparas, I. Anishchenko, N. Bennett, H. Bai, R.J. Ragotte, L.F. Milles, B.I. M. Wicky, A. Courbet, R.J. de Haas, N. Bethel, P.J.Y. Leung, T.F. Huddy, S. Pellock, D. Tischer, F. Chan, B. Koepnick, H. Nguyen, A. Kang, B. Sankaran, A.K. Bera, N. P. King, D. Baker, Robust deep learning-based protein sequence design using ProteinMPNN, Science 378 (2022) 49–56, https://doi.org/10.1126/science.add/2187
- [58] J.L. Watson, D. Juergens, N.R. Bennett, B.L. Trippe, J. Yim, H.E. Eisenach, W. Ahern, A.J. Borst, R.J. Ragotte, L.F. Milles, B.I.M. Wicky, N. Hanikel, S. J. Pellock, A. Courbet, W. Sheffler, J. Wang, P. Venkatesh, I. Sappington, S. V. Torres, A. Lauko, V. De Bortoli, E. Mathieu, S. Ovchinnikov, R. Barzilay, T. S. Jaakkola, F. DiMaio, M. Baek, D. Baker, De novo design of protein structure and function with RFdiffusion, Nature 620 (2023) 1089–1100, https://doi.org/10.1038/s41586-023-06415-8.
- [59] N. Alvisi, F.A. Gutiérrez-Mejía, M. Lokker, Y.-T. Lin, A.M. de Jong, F. van Delft, R. de Vries, Self-assembly of elastin-like polypeptide brushes on silica surfaces and nanoparticles, Biomacromolecules 22 (2021) 1966–1979, https://doi.org/ 10.1021/acs.biomac.1c00067.
- [60] D.G. Gibson, L. Young, R.-Y. Chuang, J.C. Venter, C.A. Hutchison, H.O. Smith, Enzymatic assembly of DNA molecules up to several hundred kilobases, Nat. Methods 6 (2009) 343–345, https://doi.org/10.1038/nmeth.1318.
- [61] P. Eastman, J. Swails, J.D. Chodera, R.T. McGibbon, Y. Zhao, K.A. Beauchamp, L.-P. Wang, A.C. Simmonett, M.P. Harrigan, C.D. Stern, R.P. Wiewiora, B.R. Brooks, V.S. Pande, OpenMM 7: Rapid development of high performance algorithms for

- molecular dynamics, PLoS Comput. Biol. 13 (2017), https://doi.org/10.1371/journal.pcbi.1005659 e1005659.
- [62] X. He, V.H. Man, W. Yang, T.-S. Lee, J. Wang, A fast and high-quality charge model for the next generation general AMBER force field, J. Chem. Phys. 153 (2020) 114502, https://doi.org/10.1063/5.0019056.
- [63] A. Jakalian, D.B. Jack, C.I. Bayly, Fast, efficient generation of high-quality atomic charges. AM1-BCC model: II. Parameterization and validation, J. Comput. Chem. 23 (2002) 1623–1641, https://doi.org/10.1002/jcc.10128.
- [64] D.A. Case, H.M. Aktulga, K. Belfon, D.S. Cerutti, G.A. Cisneros, V.W.D. Cruzeiro, N. Forouzesh, T.J. Giese, A.W. Götz, H. Gohlke, S. Izadi, K. Kasavajhala, M. C. Kaymak, E. King, T. Kurtzman, T.-S. Lee, P. Li, J. Liu, T. Luchko, R. Luo,
- M. Manathunga, M.R. Machado, H.M. Nguyen, K.A. O'Hearn, A.V. Onufriev, F. Pan, S. Pantano, R. Qi, A. Rahnamoun, A. Risheh, S. Schott-Verdugo, A. Shajan, J. Swails, J. Wang, H. Wei, X. Wu, Y. Wu, S. Zhang, S. Zhao, Q. Zhu, T.E. I. Cheatham, D.R. Roe, A. Roitberg, C. Simmerling, D.M. York, M.C. Nagan, K. M. Merz Jr., AmberTools, J. Chem. Inf. Model. 63 (2023) 6183–6191, https://doi.org/10.1021/acs.jcim.3c01153.
- [65] R.T. McGibbon, K.A. Beauchamp, M.P. Harrigan, C. Klein, J.M. Swails, C. X. Hernández, C.R. Schwantes, L.-P. Wang, T.J. Lane, V.S. Pande, MDTraj: a modern open library for the analysis of molecular dynamics trajectories, Biophys. J. 109 (2015) 1528–1532, https://doi.org/10.1016/j.bpj.2015.08.015.